



Cardan sequence selection influences subtalar and talonavicular joint kinematics

Anthony H. Le^a , Cassidy Knutson^b , Andrew C. Peterson^b , Bruce A. MacWilliams^{c,d} , Karen M. Kruger^{e,f} , Amy L. Lenz^{b,*}

^a Department of Biomedical Engineering, University of Utah, 36 S Wasatch Drive, Salt Lake City, UT 84112, USA

^b Department of Mechanical Engineering, University of Utah, 1495 E 100 S, Salt Lake City, UT 84112, USA

^c Department of Orthopaedics, University of Utah, 590 Wakara Way, Salt Lake City, UT 84108, USA

^d Motion Analysis Center, Shriners Hospital for Children – Salt Lake City, 1275 Fairfax Rd, Salt Lake City, UT 84103, USA

^e Department of Biomedical Engineering, Marquette University, 1515 W Wisconsin Ave, Milwaukee, WI 53233, USA

^f Motion Analysis Center, Shriners Hospital for Children – Chicago, 2211 N Oak Park Ave, Chicago, IL 60707, USA

ARTICLE INFO

Keywords:

Foot and ankle
Cardan sequences
Euler angles
Joint kinematics
Biplane fluoroscopy
Robotic cadaveric simulation

ABSTRACT

Cardan angle sequences are widely used to describe three-dimensional joint rotations in the foot and ankle, but differences in rotation order can complicate interpretation, especially in joints with multiplanar motion. This study systematically evaluated the influence of Cardan sequence selection on the kinematics of the tibiotalar, talofibular, tibiofibular, subtalar, and talonavicular joints using both *in vivo* biplane fluoroscopy gait analysis and *in vitro* passive joint kinematic data from robotic cadaveric simulation. Six Cardan sequences were evaluated to quantify their effects on joint angle profiles and range of motion. Tibiotalar, talofibular, and tibiofibular joint kinematics were largely consistent across Cardan sequences, supporting continued use of the ISB-recommended XYZ sequence (dorsiflexion/plantarflexion followed by inversion/eversion followed by internal/external rotation). Subtalar and talonavicular joint kinematics exhibited substantial sequence-dependent variations in reported joint angles during gait, prescribed tibial external/internal rotation, and prescribed tibial varus/valgus alignment motions. Sequences prioritizing the Y-axis (inversion/eversion) or Z-axis (internal/external rotation) produced the most significant differences relative to the XYZ sequence. Based on joint- and motion-specific sensitivity, we recommend the XYZ sequence for the tibiotalar, talofibular, and tibiofibular joints; YZX, XZY, or ZYX sequences for prioritizing transverse subtalar joint motion and XYZ or XZY sequences for coronal subtalar joint motion; and XYZ, XZY, or YXZ sequences for sagittal and transverse talonavicular joint motion, with YZX sequence for coronal talonavicular joint motion. These findings highlight the importance of joint-specific rotation sequence selection to improve consistency, reduce crosstalk, and enhance the clinical relevance of foot and ankle kinematic analyses.

1. Introduction

Three-dimensional (3D) joint rotations are commonly described using Euler or Cardan angle sequences. These define joint orientation or relative rigid body motions as sequential rotations about anatomically relevant axes. These methods are widely used in biomechanics due to their computational simplicity and clinical interpretability (MacWilliams and Davis, 2013; Wu and Cavanagh, 1995; Wu et al., 2002). However, because of the non-commutative nature of rotation matrices, each Cardan sequence yields a different mathematical

description of the same motion (Craig, 2006). This sequence dependency becomes particularly problematic in joints with multiplanar motion, where rotation sequence order can produce clinically or biomechanically meaningful discrepancies in reported kinematics (Phadke et al., 2011; Schache et al., 2001; Sinclair et al., 2013; Sinclair et al., 2012).

The International Society of Biomechanics (ISB) provides guidelines for reporting kinematics in the talocrural joint, but has not formally defined the bone-level local coordinate systems (LCS) or rotation sequences for the subtalar or talonavicular joints, despite their functional

* Corresponding author.

E-mail addresses: anthony.le@utah.edu (A.H. Le), kas.knutson@utah.edu (K. Knutson), andrew.c.peterson@utah.edu (A.C. Peterson), bruce.macwilliams@utah.edu (B.A. MacWilliams), karen.kruger@marquette.edu (K.M. Kruger), amy.lenz@utah.edu (A.L. Lenz).

importance (Wu et al., 2002). This gap stems partly from the historical reliance on skin marker-based motion capture, which cannot resolve bone-level joint motions (Whittaker et al., 2011). Consequently, the ISB recommendations primarily address tibiotalar motion, overlooking the talofibular and tibiofibular joints. Yet, the ankle joint complex includes a range of articulations with varying mechanical constraints, from the talocrural joint (including the tibiotalar, talofibular, and tibiofibular articulations) with greater range of motion (ROM) but fewer degrees of freedom (DOF), to the subtalar and talonavicular joints with less overall ROM but more DOF (Brockett and Chapman, 2016). These joints interact to support dynamic stability, adapt to uneven terrain, and facilitate load transfer during gait. As high-precision tools, such as biplane fluoroscopy and robotic cadaveric simulation, become more prevalent (Kessler et al., 2019; Ledoux, 2023; Natsakis et al., 2016; Wang et al., 2015; Whittaker et al., 2011), standardizing how joint motions are interpreted, particularly with respect to Cardan sequence selection, has become increasingly important.

Although prior studies have investigated rotation sequence effects in joints, such as the ankle, shoulder, and spine (Aliaj et al., 2021; Crawford et al., 1996; Phadke et al., 2011; Schache et al., 2001; Sinclair et al., 2013; Sinclair et al., 2012), few have systematically evaluated this issue across the multiple articulations of the ankle joint complex, including the subtalar and talonavicular joints. Most foot and ankle studies applied the ISB-recommended sequence corresponding to rotation about the medial-lateral axis (dorsiflexion/plantarflexion), followed by rotation about the anterior-posterior axis (inversion/eversion), followed by rotation about the superior-inferior axis (internal/external rotation) (i.e., $Ry \rightarrow Rx' \rightarrow Rz''$) or the equivalent orthogonal joint coordinate system (JCS) framework (Grood and Suntay, 1983; Wu and Cavanagh, 1995) to describe ankle joint motion (De Asla et al., 2009; Ito et al., 2015; Kobayashi et al., 2015; Kozanek et al., 2009; Lundgren et al., 2008; Maharaj et al., 2022; Okita et al., 2009; Peeters et al., 2013), and in some cases, extend the same sequence or framework to the subtalar and talonavicular joints (Conconi et al., 2024; de Asla et al., 2006; Imsdahl et al., 2020; Nester et al., 2007a; Nester et al., 2010; Nester et al., 2007b; Nichols et al., 2017; Wahl et al., 2024; Whittaker et al., 2011). While this convention may be appropriate for the talocrural joint, which exhibits quasi-planar motion in the sagittal plane, it remains unclear whether it can adequately describe the multiplanar motions in the subtalar and talonavicular joints. A comprehensive understanding of how Cardan sequence selection influences reported kinematics in these joints is critical for improving the standardization, reproducibility, and interpretability of foot and ankle biomechanics.

The purpose of this study was to systematically evaluate the influence of Cardan sequence selection on talocrural, subtalar, and talonavicular joint kinematics. Specifically, we examined the tibiotalar (TT), talofibular (TaF), tibiofibular (TiF), subtalar (ST), and talonavicular (TN) joints using both *in vivo* biplane fluoroscopy during gait and *in vitro* passive ROM data from robotic cadaveric simulation. Biplane fluoroscopy allowed us to assess sequence effects under dynamic, functional motion, while robotic cadaveric simulations enabled us to isolate these effects under controlled planar tibial rotations. We evaluated six different Cardan sequences to assess their influence on reported joint kinematics. We hypothesized that sequence selection would introduce measurable differences in joint kinematics, with greater variability expected in joints exhibiting multiplanar motion, such as the ST and TN joints.

2. Methods

2.1. In vivo biplane fluoroscopy gait analysis overview

Seven participants (6 males; 29 ± 3 yrs old; 24.7 ± 1.3 BMI) with no history of foot and ankle injury or surgery were analyzed from a previous study. Study protocol and participants recruited were under the University of Utah Institutional Review Board (IRB) approval, and all

participants gave informed consent. Participants walked barefoot at a self-selected speed over level ground. Biplane fluoroscopy image sequences were captured (Imaging Systems & Services, Inc.), and bilateral weightbearing computed tomography (WBCT) scans were obtained (pedCAT, CurveBeam AI; 120 kVp, 0.37 mm isotropic) for model-based markerless tracking (Perez et al., 2024).

2.2. Cadaveric passive range of motion testing overview

Five fresh-frozen tibia-to-toe tip cadaveric specimens (5 males; 53 ± 13 yrs old; 24.4 ± 3.2 BMI) with no history of foot and ankle injury or surgery were analyzed from a previous study (Le et al., 2025). Specimens were procured under University of Utah IRB approval. Conventional fan-beam CT scans were acquired (SOMATOM Force, Siemens Medical Solutions; 120 kVp, 100 mAs, 0.6 mm isotropic) and segmented to generate full-length tibia and fibula bone models in Mimics v26.0 (Mimics Innovation Suite, Materialise). Specimen-specific 3D-printed molds rigidly affixed the proximal tibia to a 6-axis industrial robot (M-20iA, FANUC America), while allowing free fibular motion. Tibia LCS was defined at the tibiotalar joint center as the robot's tool center point (i.e., center of rotation) using our lab's open-source Automatic Anatomical Foot and Ankle Coordinate Toolbox (AAFACT) and a cylinder fit to the tibial plafond (Knutson et al., 2024; Lenz et al., 2021; Muhlrad et al., 2024; Peterson et al., 2023) (Fig. 1).

Infrared marker clusters were attached to the tibia, fibula, talus, calcaneus, and navicular bones via custom radiopaque 3D-printed bone pins. Rigid body motion of each marker was tracked in 6 DOF (3 translations and 3 rotations) at 250 Hz using an active optical motion capture system (Optotrak Certus, NDI) and represented with 4×4 homogeneous transformation matrices.

Tibial rotation endpoints were determined through a motion profile tuning procedure to define specimen-specific tibial ROM in the sagittal, transverse, and coronal planes (Le et al., 2025). During passive ROM testing, each specimen was loaded to $25 \pm 2.5\%$ body weight (BW) at 1 mm/s in a neutral position on a flat surface and robotically prescribed tibial dorsiflexion/plantarflexion (DF/PF), tibial external/internal rotation (ER/IR), and tibial varus/valgus alignment (VR/VG) at $2^\circ/\text{s}$ (2 Hz) to their respective tibial ROM endpoints.

2.3. Data processing

For *in vivo* gait kinematics, WBCT scans were segmented to generate 3D reconstructions of the tibia, fibula, talus, calcaneus, and navicular using a semi-automatic segmentation software (Bonenlogic Ortho Foot & Ankle v2.1.1, DISIOR) and Mimics v26.0 (Mimics Innovation Suite, Materialise). Bone-level 3D orientations and translations in each frame of the biplane fluoroscopy recordings were computed using a previously described and validated model-based markerless tracking pipeline in DSX (HAS-Motion) (Perez et al., 2024).

For cadaveric passive kinematics, cone beam CT scans of each cadaveric specimen with radiopaque 3D-printed bone pins attached to the tibia, fibula, talus, calcaneus, and navicular were segmented using Bonelogic and Mimics v26.0. Transformation matrices registering marker cluster LCS to bone LCS for each bone were calculated using the object registration and transformation matrix functions in 3-Matic v18.0 (Mimics Innovation Suite, Materialise). These marker-to-bone-specific transformation matrices were used to transform rigid body marker motion into rigid body bone motion.

Bone-level LCS for the tibia, fibula, talus, calcaneus, and navicular were defined using AAFACT (Peterson et al., 2023) (Fig. 1). The talus had multiple articular relationships that were accounted for by defining different LCS specific to its joint relationship with the tibia, calcaneus, and navicular (i.e., TT vs ST vs TN, respectively). TT, TaF, TiF, ST, and TN joint rotations for each participant and cadaveric specimen were calculated from the transformation matrices via Euler decomposition and Cardan sequences and normalized to initial joint angles measured in

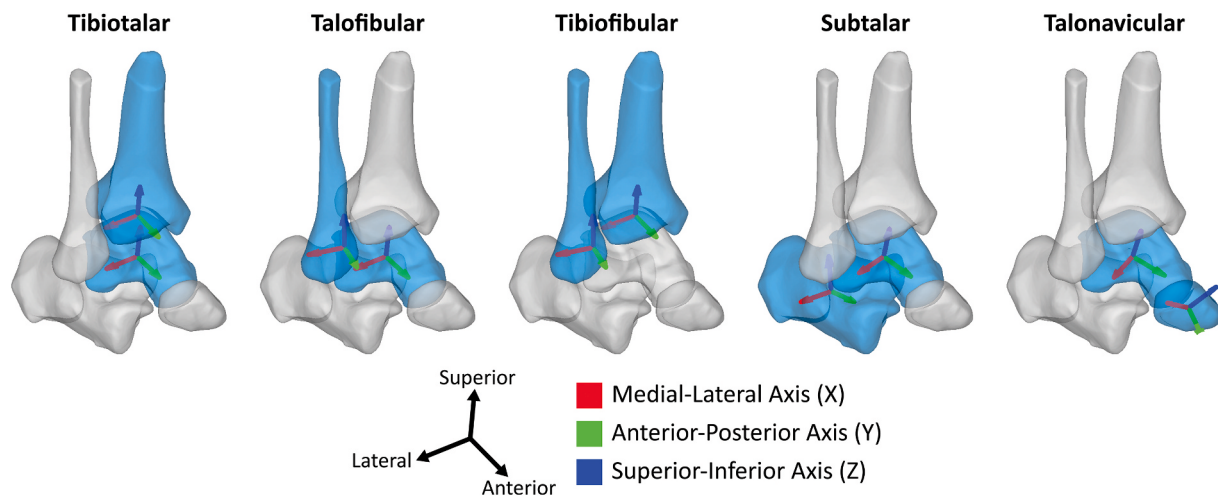


Fig. 1. Bone-level local coordinate systems for the tibiotalar, talofibular, tibiofibular, subtalar, and talonavicular joints of a right ankle joint complex in a neutral position. Coordinate systems were defined using our lab's open-source Automatic Anatomical Foot and Ankle Coordinate Toolbox (AAFACT). X-axis (red) as the medial-lateral axis, Y-axis (green) as the anterior-posterior axis, and Z-axis (blue) as the superior-inferior axis.

the loaded, neutral position on the flat surface.

Cardan sequences refer to a specific type of rotation sequence used in calculating 3D joint kinematics and strictly involve rotations about 3 different axes (Grood and Suntay, 1983; MacWilliams and Davis, 2013; Wu and Cavanagh, 1995; Wu et al., 2002). All joint motion data were calculated using the XYZ, XZY, YXZ, YZX, ZXY, and ZYX Cardan rotation sequences using a custom MATLAB script and the built-in rot2eul MATLAB function (MATLAB R2024b, MathWorks). X-axis was defined as the medial-to-lateral direction, Y-axis as the posterior-to-anterior direction, and Z-axis as the inferior-to-superior direction, consistent with the right-hand rule. The ISB-recommended $Ry \rightarrow Rx' \rightarrow Rz'$ sequence for lower limb kinematics (Wu et al., 2002) is equivalent to the XYZ sequence used in this study, where rotations are performed sequentially about the X-axis (i.e., dorsiflexion/plantarflexion (DF/PF) or sagittal plane motion), followed by the Y-axis (i.e., inversion/eversion (INV/EV) or coronal plane motion), followed by the Z-axis (i.e., internal/external rotation (IR/ER) or transverse plane motion).

2.4. Statistical analysis

One-way ANOVA temporal statistical parametric mapping (SPM) analysis ($\alpha = 0.05$) was used to compare individual joint rotations across Cardan sequences, followed by post hoc pairwise comparisons with Bonferroni correction for parametric data or post hoc non-parametric permutation testing for non-parametric data (Nichols and Holmes, 2002) at each instance of normalized percent activity using the MATLAB-based spm1d package (Pataky, 2010; Pataky et al., 2013, 2016; Pataky et al., 2015).

Mean ROM at each joint across Cardan sequences was compared using one-way ANOVA, followed by Tukey HSD post hoc pairwise comparisons for parametric ROM data or Kruskal-Wallis analysis with Dunn-Sidak Correction for non-parametric ROM data using a custom MATLAB script (MATLAB R2024b, MathWorks). Significance level was set a priori at $\alpha = 0.05$. Normality was assessed with the Shapiro-Wilk test, and homogeneity of variance was assessed with the Levene test. For conciseness, only pairwise comparisons with respect to XYZ were reported.

3. Results

3.1. Gait kinematics

During stance, SPM analysis revealed no significant differences in

TT, TaF, or TiF joint kinematics between XYZ and any other Cardan sequence (Fig. 2). However, YZX, ZXY, and ZYX increased ST eversion (EV) and TN inversion (INV) during specific portions of stance compared to XYZ, while YZX increased TN ER compared to XYZ (Fig. 2).

Despite these directional differences in kinematic profiles, the overall ROM during the stance was not significantly different between XYZ and any other Cardan sequence across all joints (Fig. 3).

3.2. Cadaveric passive range of motion kinematics

3.2.1. Prescribed tibial dorsiflexion/plantarflexion (DF/PF) motion

During prescribed tibial DF/PF, YZX, ZXY, and ZYX sign-inverted the passive coronal TaF kinematics relative to XYZ. Similarly, YXZ sign-inverted the passive transverse TaF kinematics relative to XYZ (Fig. 4). XZY, ZXY, and ZYX increased passive TN DF during the transition period between peak prescribed tibial DF and PF and increased passive TN PF, compared to XYZ during peak prescribed tibial PF (Fig. 4).

Regarding overall passive ROM, YZX, ZXY, and ZYX increased passive coronal TaF ROM compared to XYZ (Fig. 5). XZY and ZXY increased passive sagittal ST ROM, while YXZ increased passive transverse ST ROM compared to XYZ (Fig. 5).

3.2.2. Prescribed tibial external/internal rotation (ER/IR) motion

During prescribed tibial ER/IR, XZY, ZXY, and ZYX sign-inverted the passive sagittal TN kinematics, while YZX, ZXY, and ZYX amplified passive coronal TN kinematics relative to XYZ (Fig. 6).

Although there were no differences in the kinematic profiles of the ST joint between XYZ and any other Cardan sequence, specific differences in the overall ROM were observed: XZY increased passive sagittal ST ROM; YZX, ZXY, and ZYX decreased passive coronal ST ROM; and YXZ, YZX, and ZYX increased passive transverse ST ROM compared to XYZ (Fig. 7). Additionally, ZXY increased passive sagittal TN ROM, YZX, ZXY, and ZYX increased passive coronal TN ROM, and YZX decreased passive transverse TN ROM compared to XYZ (Fig. 7).

3.2.3. Prescribed tibial varus/valgus (VR/VG) alignment motion

During prescribed tibial VR/VG, XZY, ZXY, and ZYX amplified sagittal ST kinematics, while YXZ, YZX, ZXY, and ZYX reduced coronal ST, but amplified transverse ST kinematics compared to XYZ (Fig. 8). XZY, ZXY, and ZYX sign-inverted the sagittal TN kinematics, whereas YXZ and YZX decreased sagittal TN kinematics compared to XYZ. XZY, YXZ, YZX, ZXY, and ZYX amplified coronal TN kinematics, while YXZ, YZX, and ZYX reduced transverse TN kinematics compared to XYZ.

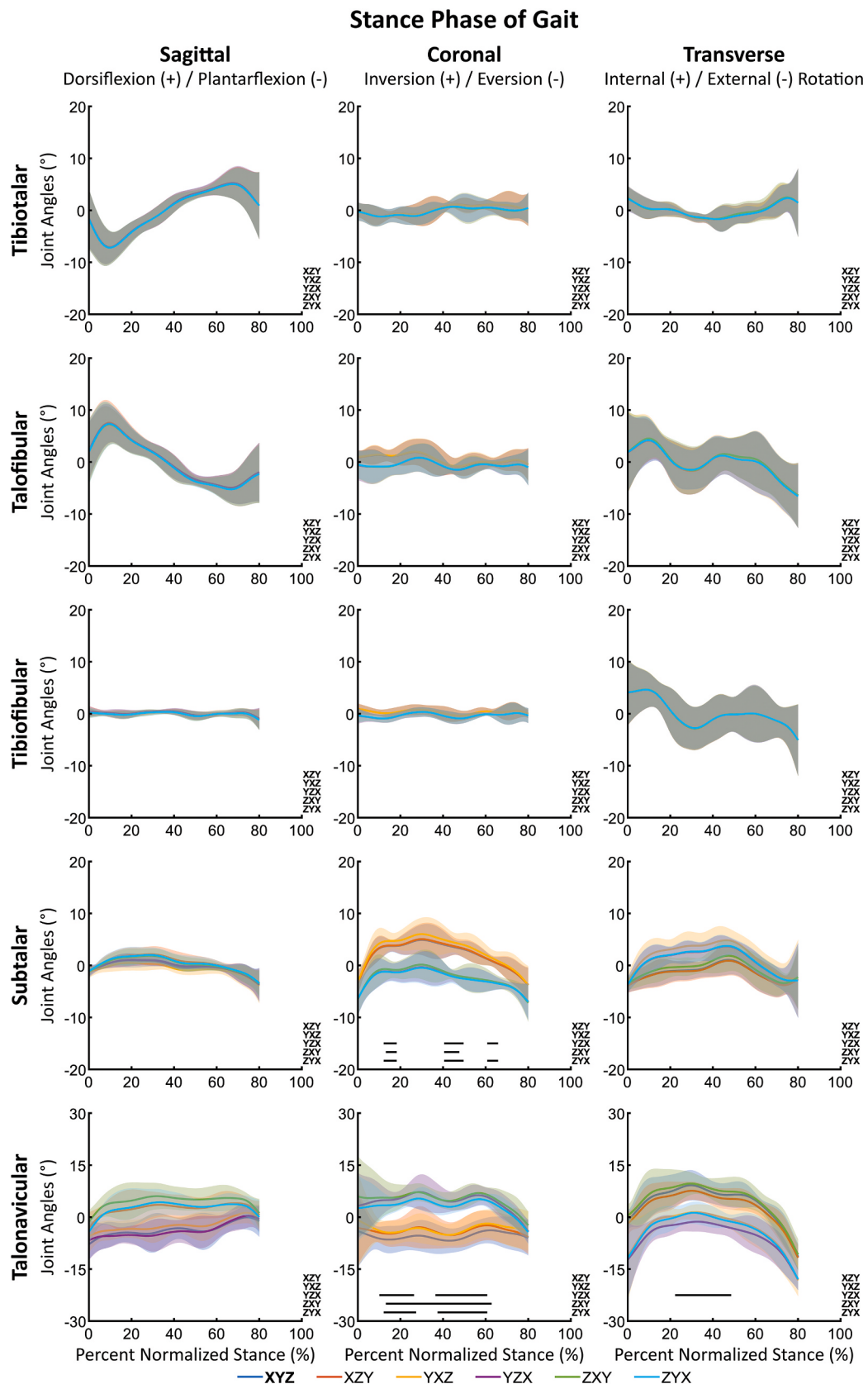


Fig. 2. Mean (\pm SD) tibiotalar, talofibular, tibiofibular, subtalar, and talonavicular joint kinematics in the sagittal, coronal, and transverse plane during the stance phase of gait for each Cardan sequence. Black horizontal bars indicate portions of the stance phase of gait where joint kinematics were significantly different between XYZ (dorsiflexion/plantarflexion followed by inversion/eversion followed by internal/external rotation) and other Cardan sequences ($\alpha < 0.05$).

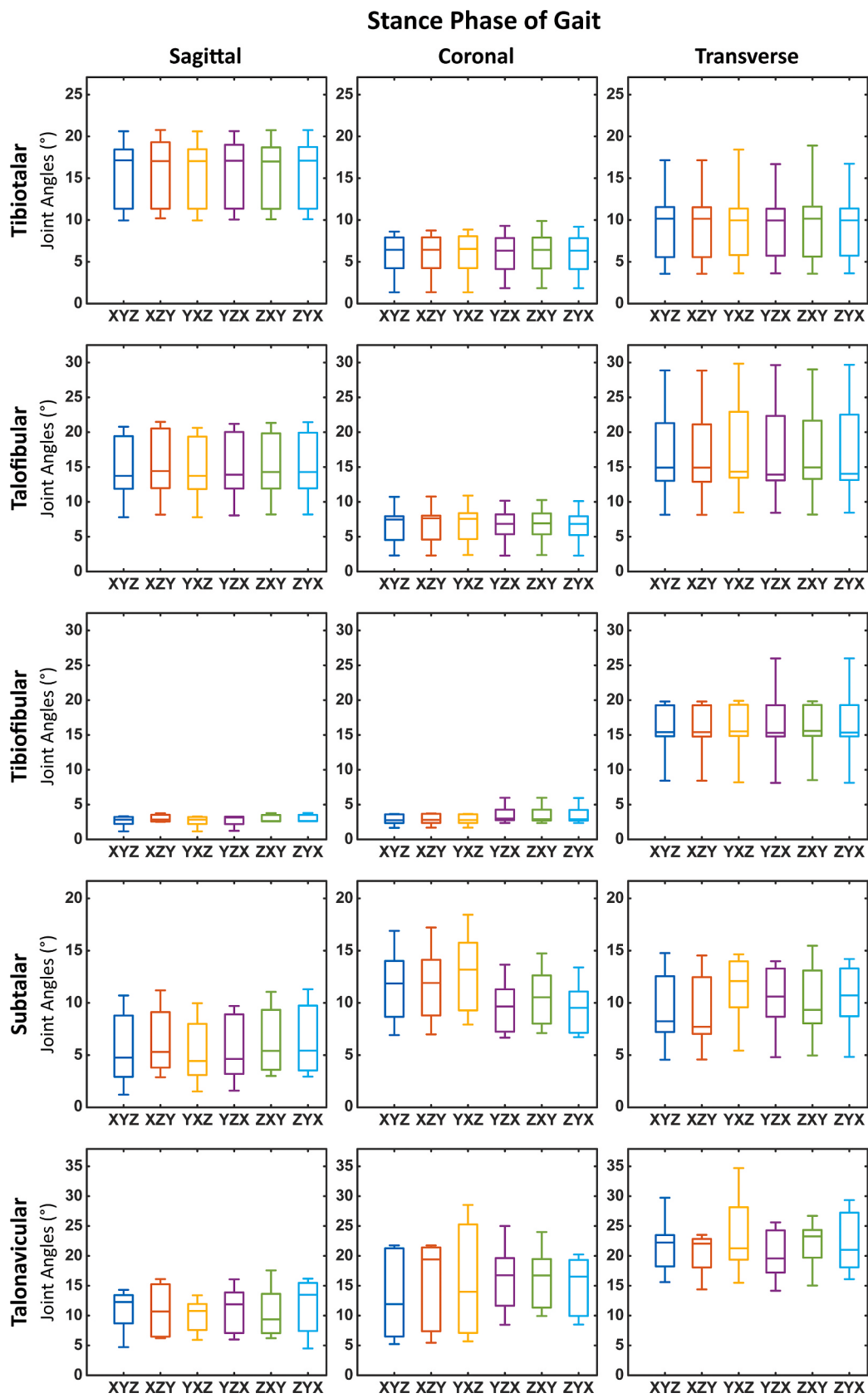


Fig. 3. Mean (\pm SD) tibiotalar, talofibular, tibiofibular, subtalar, and talonavicular joint range of motion in the sagittal, coronal, and transverse plane during the stance phase of gait for each Cardan sequence. Asterisk (*) indicate a significant difference between XYZ (dorsiflexion/plantarflexion followed by inversion/eversion followed by internal/external rotation) and other Cardan sequences ($\alpha < 0.05$).

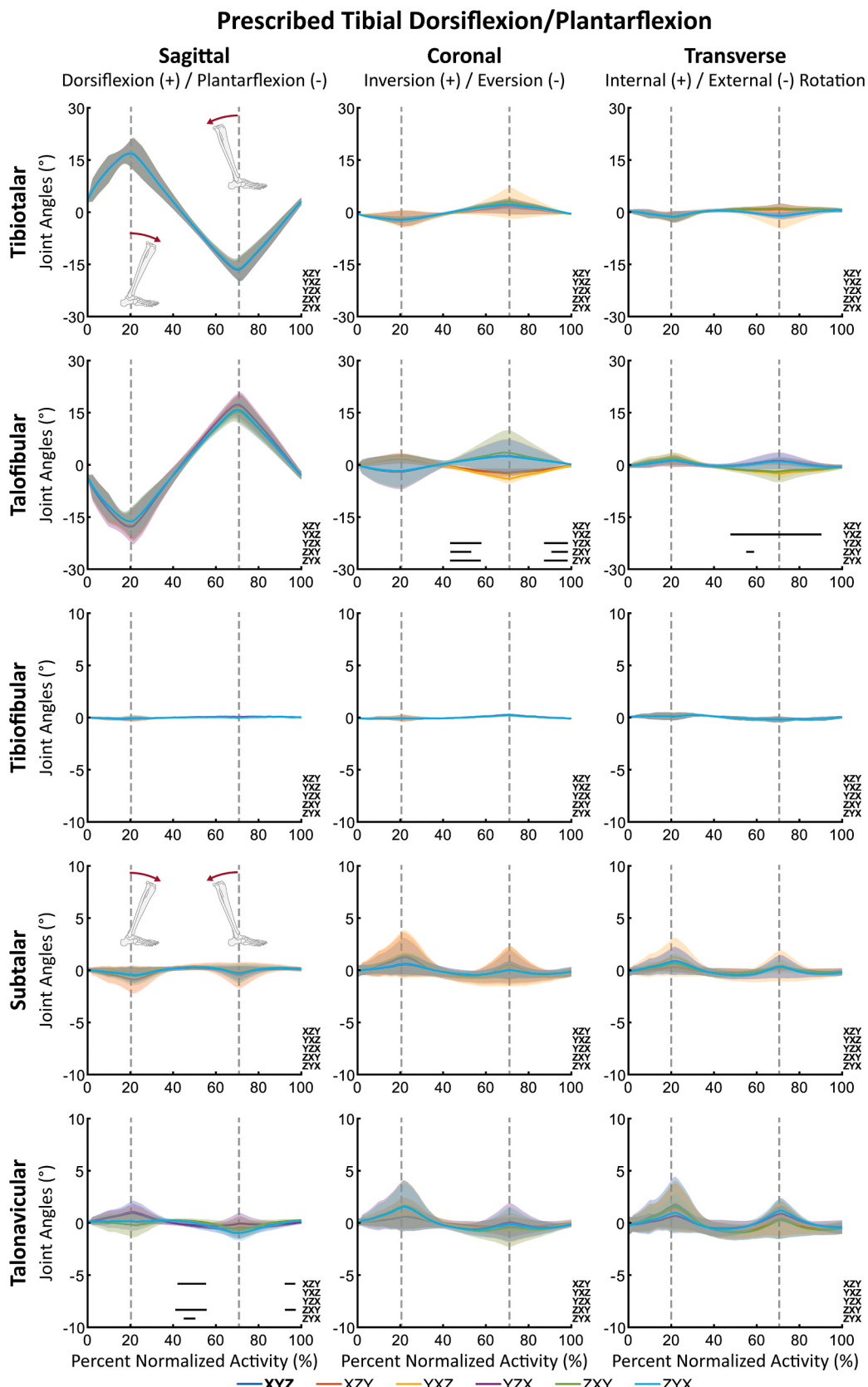


Fig. 4. Mean (\pm SD) tibiotalar, talofibular, tibiofibular, subtalar, and talonavicular joint kinematics in the sagittal, coronal, and transverse plane during prescribed tibial dorsiflexion/plantarflexion motion for each Cardan sequence. Black horizontal bars indicate portions of prescribed motion where joint kinematics were significantly different between XYZ (dorsiflexion/plantarflexion followed by inversion/eversion followed by internal/external rotation) and other Cardan sequences ($\alpha < 0.05$). First grey vertical dashed line indicates peak prescribed dorsiflexion. Second grey vertical dashed line indicates peak prescribed plantarflexion.

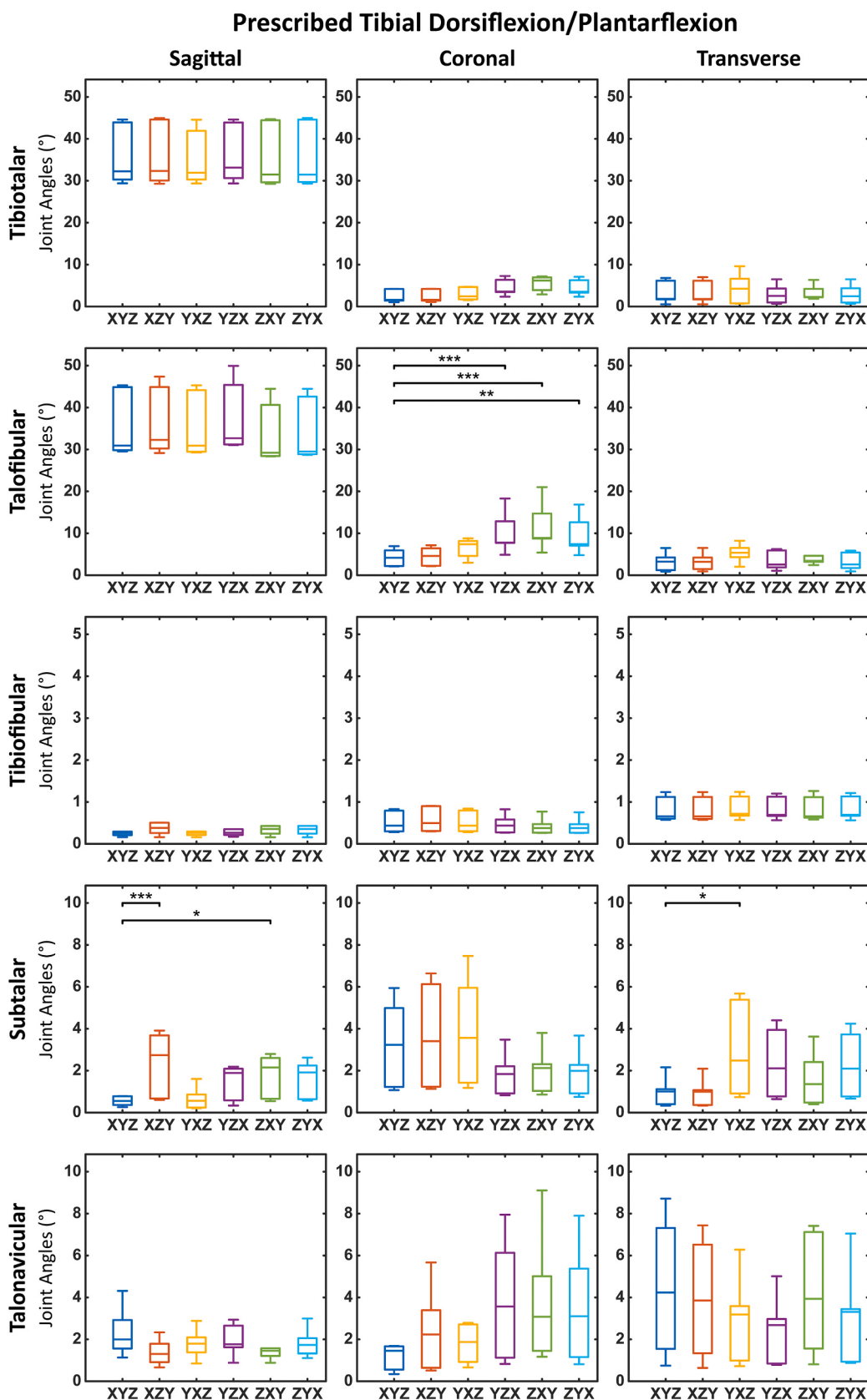


Fig. 5. Mean (\pm SD) tibiotalar, talofibular, tibiofibular, subtalar, and talonavicular joint range of motion in the sagittal, coronal, and transverse plane during prescribed tibial dorsiflexion/plantarflexion motion for each Cardan sequence. Asterisk (*) indicate a significant difference between XYZ (dorsiflexion/plantarflexion followed by inversion/eversion followed by internal/external rotation) and other Cardan sequences ($\alpha < 0.05$).

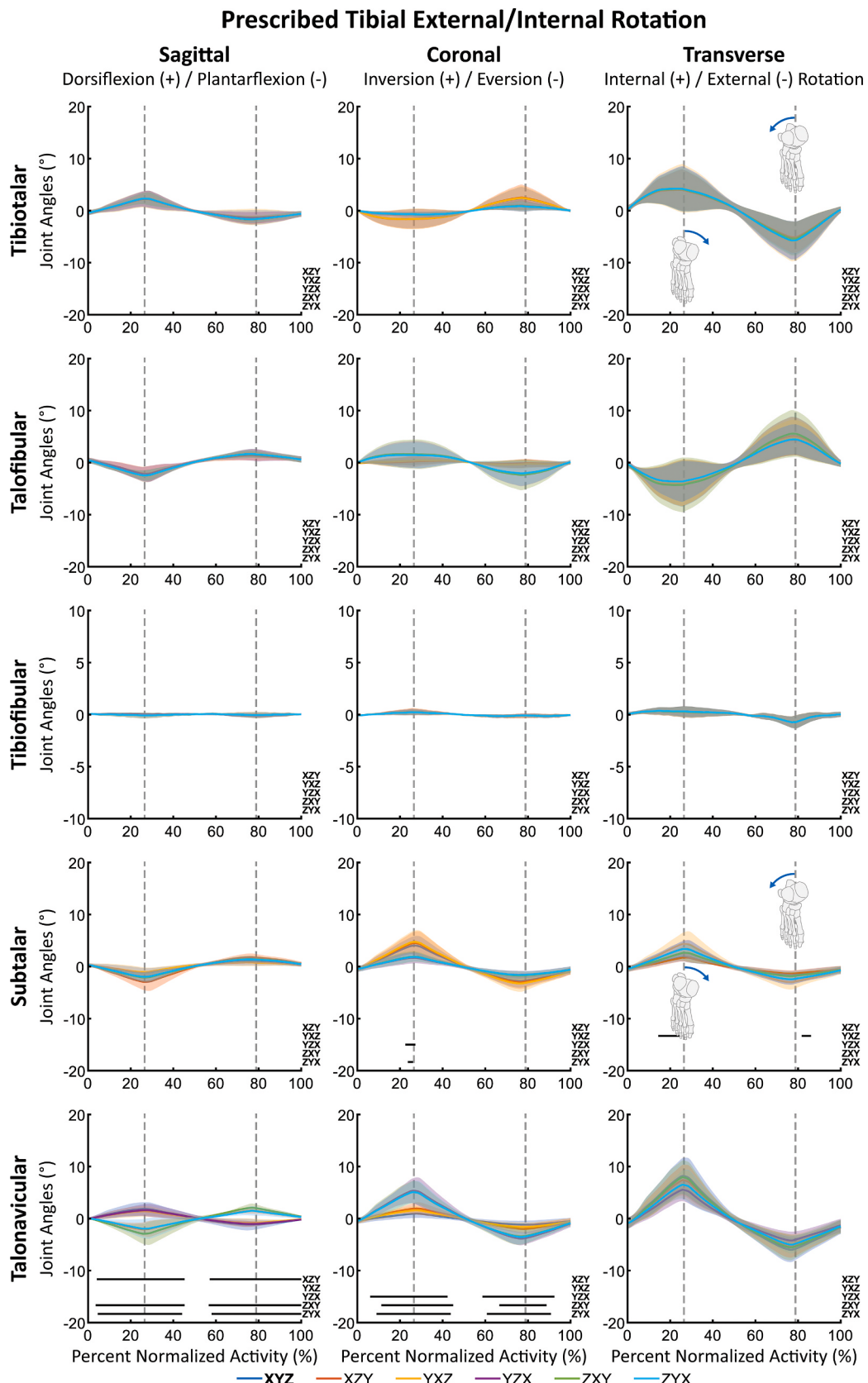


Fig. 6. Mean (\pm SD) tibiotalar, talofibular, tibiofibular, subtalar, and talonavicular joint kinematics in the sagittal, coronal, and transverse plane during prescribed tibial external/internal rotation motion for each Cardan sequence. Black horizontal bars indicate portions of prescribed motion where joint kinematics were significantly different between XYZ (dorsiflexion/plantarflexion followed by inversion/eversion followed by internal/external rotation) and other Cardan sequences ($\alpha < 0.05$). First grey vertical dashed line indicates peak prescribed tibial external rotation. Second grey vertical dashed line indicates peak prescribed tibial internal rotation.

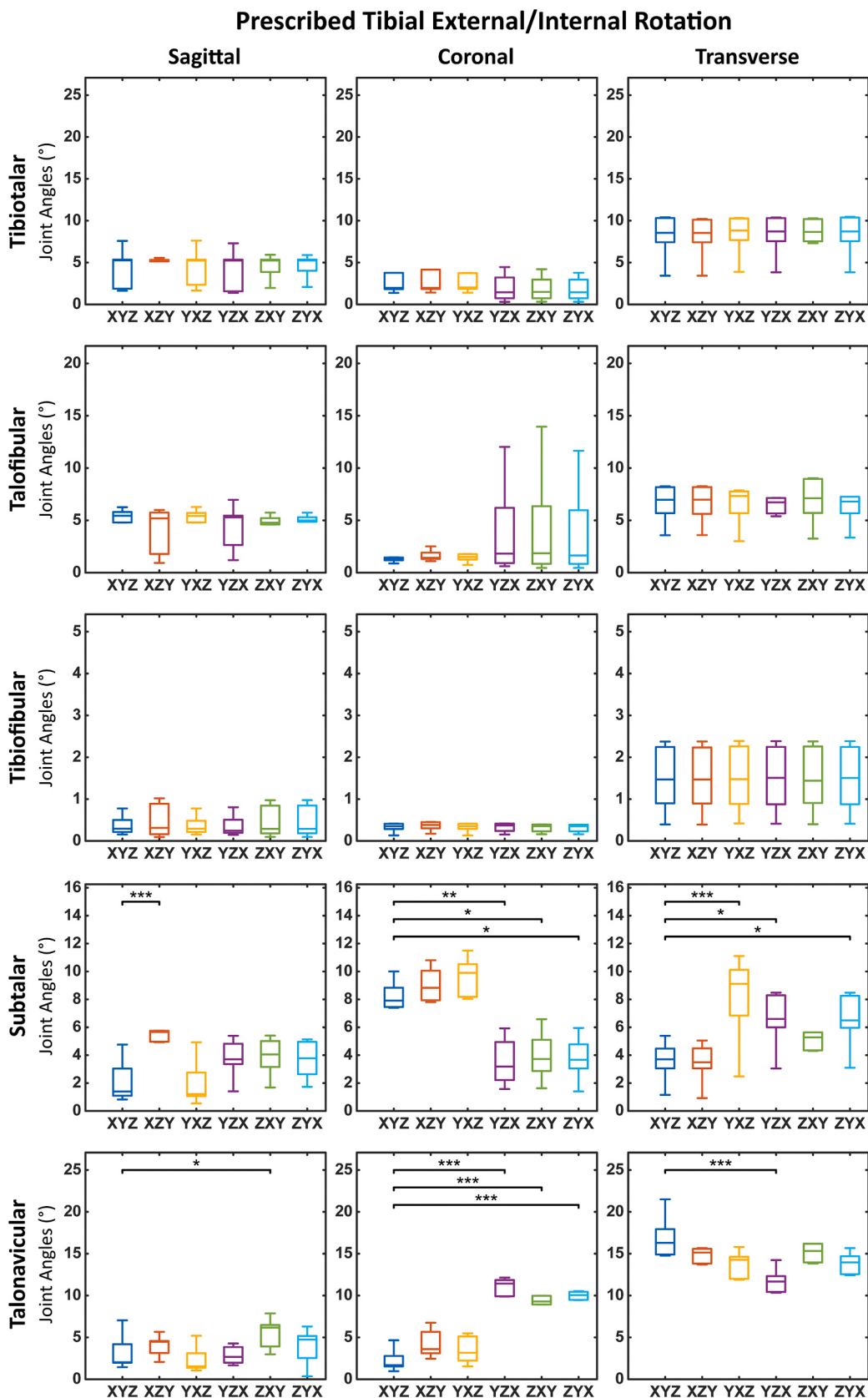


Fig. 7. Mean (\pm SD) tibiotalar, talofibular, tibiofibular, subtalar, and talonavicular joint range of motion in the sagittal, coronal, and transverse plane during prescribed tibial external/internal rotation motion for each Cardan sequence. Asterisk (*) indicate a significant difference between XYZ (dorsiflexion/plantarflexion followed by inversion/eversion followed by internal/external rotation) and other Cardan sequences ($\alpha < 0.05$).

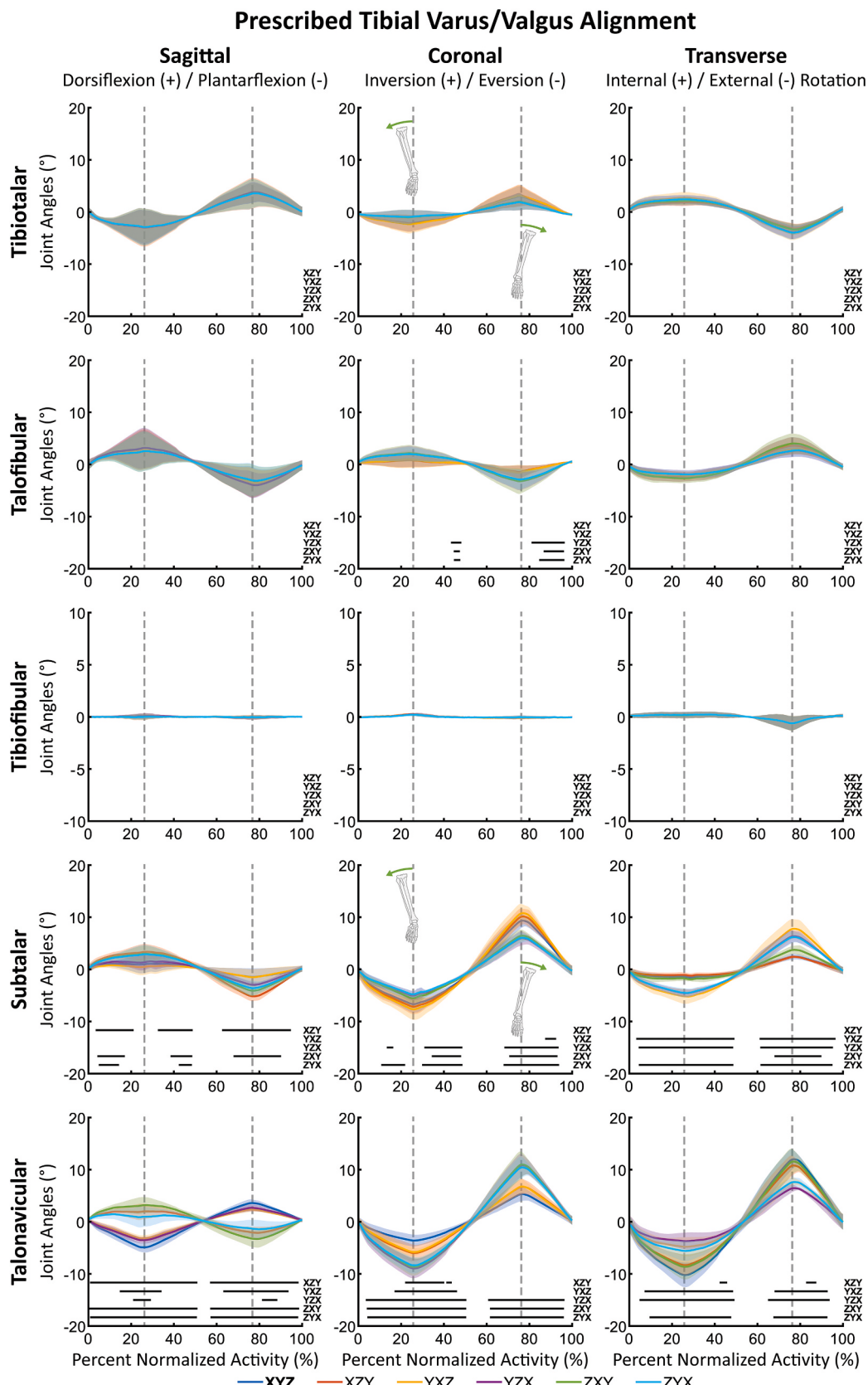


Fig. 8. Mean (\pm SD) tibiotalar, talofibular, tibiofibular, subtalar, and talonavicular joint kinematics in the sagittal, coronal, and transverse plane during prescribed tibial varus/valgus alignment motion for each Cardan sequence. Black horizontal bars indicate portions of prescribed motion where joint kinematics were significantly different between XYZ (dorsiflexion/plantarflexion followed by inversion/eversion followed by internal/external rotation) and other Cardan sequences ($\alpha < 0.05$). First grey vertical dashed line indicates peak prescribed varus alignment. Second grey vertical dashed line indicates peak prescribed valgus alignment.

(Fig. 8).

Regarding overall passive ROM, YZX increased passive coronal TaF ROM compared to XYZ (Fig. 9). XZY, ZXY, ZYX increased passive sagittal ST ROM; YZX, ZXY, and ZYX decreased passive coronal ST ROM; and YXZ, YZX, and ZYX increased passive transverse ST ROM compared to XYZ (Fig. 9). XZY, YXZ, and ZYX decreased passive sagittal TN ROM; YZX, ZXY, and ZYX increased passive coronal TN ROM; and YXZ, YZX, and ZYX decreased passive transverse TN ROM compared to XYZ (Fig. 9).

4. Discussion

This study systematically evaluated the influence of Cardan sequence selection on talocrural, ST, and TN joint kinematics and ROM using both *in vivo* biplane fluoroscopy and *in vitro* robotic cadaveric simulations. These complementary datasets enabled us to characterize sequence-dependent differences in functional and controlled conditions. Biplane fluoroscopy provided insight into sequence-dependent differences during level-ground walking, while robotic cadaveric simulations isolated differences in joint angles attributable solely to sequence choice. Both approaches leveraged high-precision motion capture techniques for bone-level joint kinematics.

Consistent with our hypothesis, Cardan sequence selection was joint- and motion-dependent. The TT, TaF, and TiF joints exhibited minimal variation in joint angle profiles and overall ROM across Cardan sequences relative to XYZ (DF/PF followed by INV/EV followed by IR/ER) during gait and prescribed planar tibial motions. This supports the notion that sequence effects are negligible in joints with predominantly quasi-planar motion, where their limited DOF, dominant sagittal plane motion, and minimal coronal and transverse contributions reduce the potential for crosstalk (Areblad et al., 1990; Novacheck, 1998; Thewlis et al., 2008). These results align with prior studies showing that XYZ is most appropriate for describing ankle joint kinematics during walking and cycling (Sinclair et al., 2013; Sinclair et al., 2012).

In contrast, the ST and TN joints demonstrated pronounced sensitivity to Cardan sequence selection, particularly during gait and prescribed tibial ER/IR and VR/VG motions. The most significant deviations from XYZ were observed in sequences that prioritized rotation about the Y-axis (inversion/eversion) or Z-axis (internal/external rotation). This sensitivity likely reflects the multiplanar kinematics, oblique joint orientations, and greater DOF of these joints, where dominant motions do not align neatly with a single anatomical plane (Fig. 10). When the dominant motion of a joint is placed later in a rotation sequence, preceding rotations can reorient the anatomical axes, causing portions of the intended motion to project into non-dominant planes. This effect is commonly referred to as crosstalk. Conversely, placing the dominant plane of motion earlier in the sequence helps preserve its alignment with anatomical axes and reduces such artifacts. These principles explain why sequences, such as YZX or ZYX, which begin with rotations in the coronal or transverse planes, may reduce crosstalk in the ST and TN joints and yield more interpretable representations of their kinematics. Similar sequence-dependent discrepancies have been observed in other anatomically complex joints, such as the shoulder and spine (Phadke et al., 2011; Schache et al., 2001).

Notably, the ST joint has demonstrated considerable inter-subject variability in its dominant plane of motion. Although it is typically described as exhibiting primarily coronal and transverse plane motion, subject-level analyses have shown that some individuals display greater sagittal than transverse motion during gait (Lundgren et al., 2008). In contrast, the TN joint consistently displays coronal and transverse plane motion during activities, such as walking, tibial ER/IR, and pronation/supination (Lundberg and Svensson, 1993; Lundgren et al., 2008; Nester et al., 2002; Sammarco, 2004; Sarrafian, 1993). Its ball-and-socket-like morphology affords greater DOF, amplifying the impact of sequence rotation ordering on reported joint kinematics (Nester et al., 2001; Tweed et al., 2008).

Our findings reinforce these anatomical and functional distinctions. Specifically, YZX, ZXY, and ZYX consistently produced greater eversion at the ST joint and greater INV and ER at the TN joint compared to XYZ during gait (Fig. 2). Although overall ROM was similar across sequences (Fig. 3), these directional discrepancies in the coronal and transverse planes could influence interpretations of joint function. While gait is generally sagittal-plane dominant, the ST and TN joints contribute more through coronal and transverse motions (Fig. 3). Thus, sequences prioritizing these planes may yield more physiologically relevant representations during walking.

Sequence-related differences were further amplified in robotic cadaveric simulations, where planar tibial motion inputs allowed isolation of sequence effects. During prescribed tibial ER/IR, when transverse joint motion is expected to be emphasized, YZX, ZXY, and ZYX increased transverse ROM while decreasing coronal ROM in the ST joint relative to XYZ (Fig. 7). In contrast, these same sequences increased coronal ROM while maintaining similar transverse ROM in the TN joint (Fig. 7). This suggests they may improve interpretability for the ST joint in this context, but may not be necessary for the TN joint.

During prescribed tibial VR/VG, where coronal motion is the primary expected response, XYZ and XZY yielded greater coronal and lower transverse ROM in the ST joint compared to YZX, ZXY, and ZYX, aligning better with the intended motion (Fig. 9). YXZ, however, exaggerated both coronal and transverse ROM in the ST joint, which may reflect increased crosstalk (Fig. 9). In the TN joint, YZX increased coronal ROM while decreasing transverse ROM compared to XYZ, suggesting it may be better for evaluating coronal plane motion in this joint.

Altogether, these findings highlight the risk of misinterpretation when applying a single rotation sequence (e.g., XYZ) across all joints in the foot and ankle with varying mechanical behaviors and motion characteristics. While our results support the need for joint-specific considerations, they do not conclusively validate or invalidate any one sequence for all joints, particularly for the ST joint, where complex anatomy and variability in motion during gait limit clear recommendations. Conversely, the TN joint showed more consistent trends, supporting sequences aligned with dominant motion planes to reduce crosstalk and improve kinematic interpretability.

Given the widespread adoption of the ISB-recommended XYZ sequence for the hip, knee, and ankle (Wu et al., 2002), our results support its continued use for the TT, TaF, and TiF joints, where motion is predominantly planar and sequence sensitivity is minimal. However, alternative sequences may offer more interpretable joint- or motion-specific representations for joints with greater DOF and multiplanar kinematics, such as the ST and TN joints. Therefore, we propose the following recommendations: (1) for TT, TaF, and TiF joint kinematics, we recommend continued use of XYZ (DF/PF followed by INV/EV followed by IR/ER); (2) for ST joint kinematics, we recommend the use of YZX, ZXY, or ZYX when transverse plane motion is of primary interest and XYZ or XZY when analyzing coronal plane motion; and (3) for TN joint kinematics, we recommend XYZ, XZY, or YXZ for evaluating sagittal and transverse plane motion, while YZX is recommended when coronal plane motion is of interest. These recommendations aim to provide more physiologically and clinically interpretable results, minimize directional artifacts, reduce kinematic crosstalk, and support more accurate comparative analyses across studies. However, we recognize that this is a complex problem with no one-size-fits-all solution. The findings of this study suggest that the optimal sequence selection is inherently both joint- and motion-specific and should be guided by the dominant plane(s) of interest and intended biomechanical interpretation.

This study has several limitations. First, while biplane fluoroscopy and robotic cadaveric simulations provide highly accurate bone-level kinematics, the sample sizes were modest. Larger, more diverse datasets with pathological conditions may reveal additional nuances in sequence sensitivity. However, our sample sizes are consistent with prior studies using these resource-intensive techniques, and the

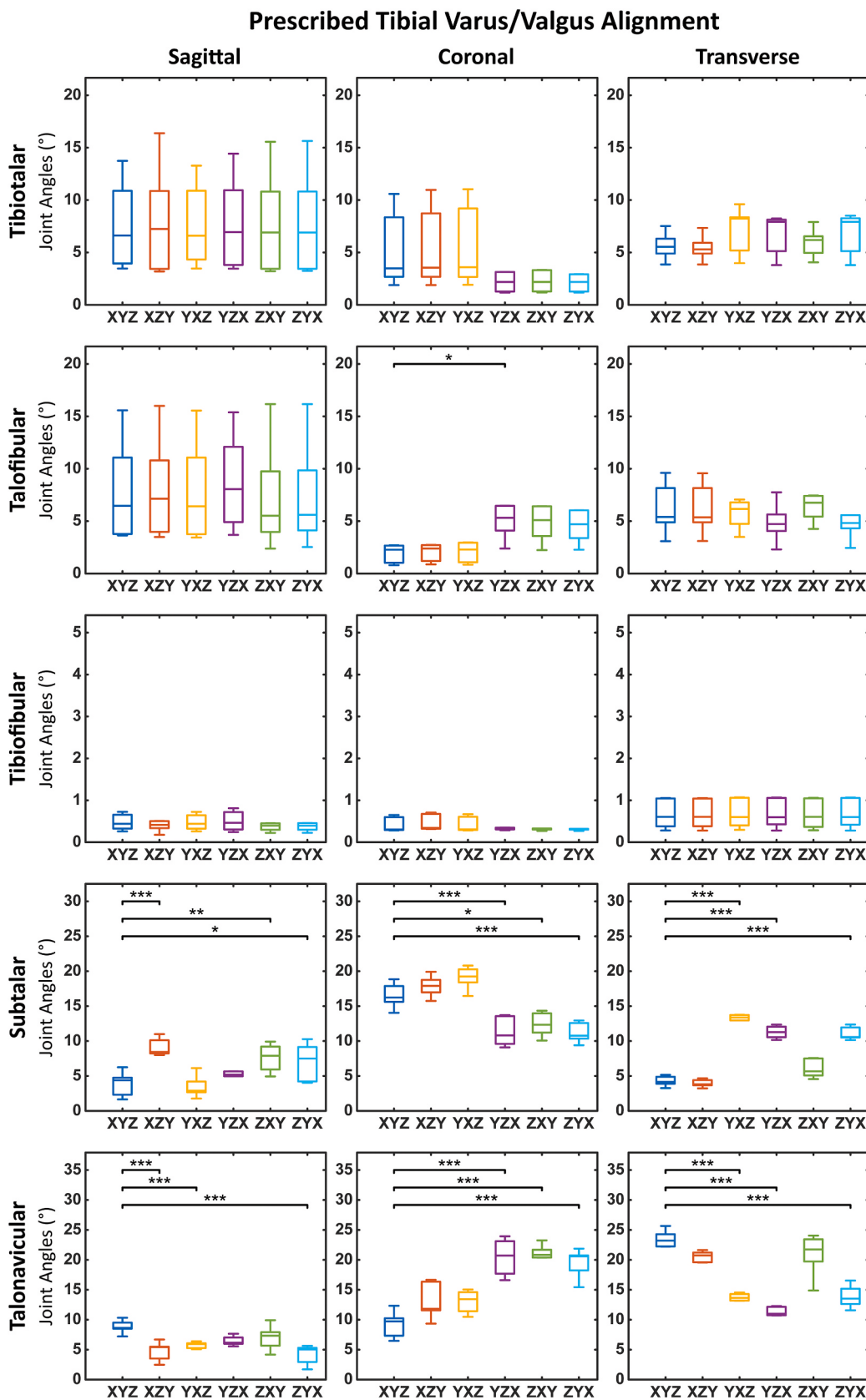


Fig. 9. Mean (\pm SD) tibiotalar, talofibular, tibiofibular, subtalar, and talonavicular joint range of motion in the sagittal, coronal, and transverse plane during prescribed tibial varus/valgus alignment motion for each Cardan sequence. Asterisk (*) indicate a significant difference between XYZ (dorsiflexion/plantarflexion followed by inversion/eversion followed by internal/external rotation) and other Cardan sequences ($\alpha < 0.05$).

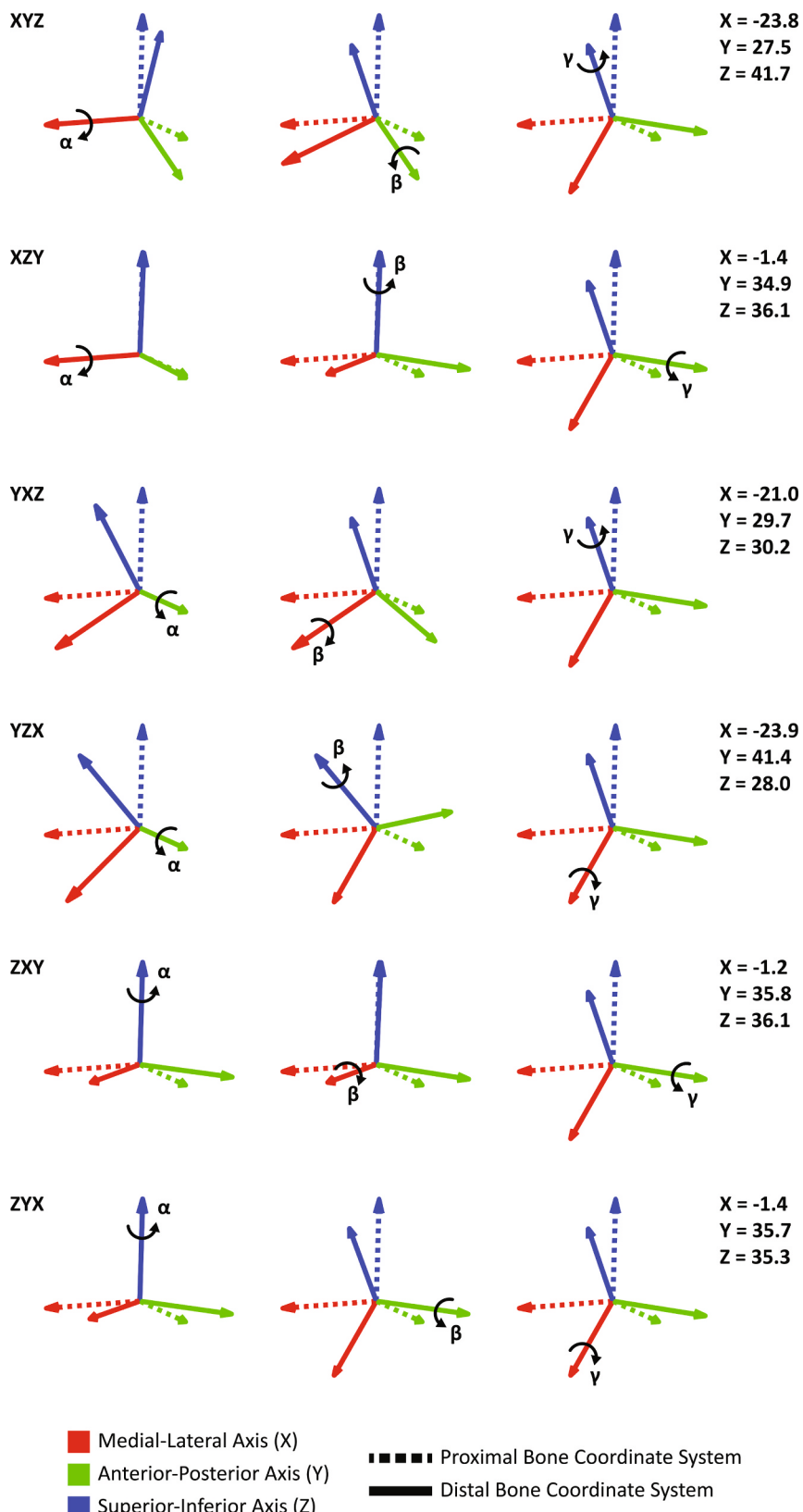


Fig. 10. Representative Euler angle decomposition using each Cardan sequence (XYZ, XZY, YXZ, YZX, ZXY, and ZYX) for the talonavicular joint at a single time point during the stance phase of gait. Joint angles are calculated by expressing the distal segment local coordinate system relative to the proximal segment local coordinate system. Euler decomposition yields three successive angles, denoted α , β , and γ , corresponding to the first, second, and third rotations in the specified Cardan sequence. Rotations are expressed relative to anatomical axes: X-axis (red) as the medial-lateral axis (dorsiflexion (+)/plantarflexion (-) angle), Y-axis (green) as the anterior-posterior axis (inversion (+)/eversion (-) angle), and Z-axis (blue) as the superior-inferior axis (internal (+)/external (-) rotation angle).

application of temporal SPM enabled robust statistical analysis of one-dimensional joint angle trajectories despite the small sample size. SPM accounts for temporal smoothness and controls for family-wise error rate, and we further employed non-parametric permutation testing when appropriate to ensure statistical validity. The consistency of trends observed across both *in vivo* and *in vitro* datasets strengthens our confidence in the robustness of the findings. Second, our analysis was restricted to six commonly used Cardan sequences. While this offers practical relevance, alternative representations such as helical axes or quaternion interpolations were not evaluated. Although helical axes have shown promise for characterizing hindfoot motion (Behling et al., 2024; Behling et al., 2025), their clinical interpretability remains limited, and thus they were excluded from this analysis. Third, cadaveric simulations allowed us to isolate tibial input, but the current analysis lacked muscle forces and soft tissue contributions that modulate joint motion *in vivo*. Lastly, we recognize that many clinical and research applications involve interest in multiple planes of motion simultaneously, and that optimal sequence choice in such cases remains unresolved. As such, the recommendations outlined above reflect relative trade-offs based on which motion plane is prioritized.

Future work should establish consensus around primary motion directions in complex joints, like the ST and TN joints, during gait to guide more consistent rotation sequence selection. Future investigations should also explore additional joints (e.g., calcaneocuboid and naviculocuneiform), especially under pathological gait conditions, like cerebral palsy, flatfoot, or joint instability, where kinematic interpretations are more critical (Henry et al., 2022). These conditions may shift the dominant planes of motion and alter joint behavior, which could further complicate interpretation of joint angles. Extending this analysis to pathological populations will be essential for translating our findings into clinically meaningful recommendations. While level-ground walking is a representative activity of daily living, it may not challenge the full ROM or complexity of the talocrural, ST, and midtarsal joints. Including activities that involve more dynamic, multiplanar joint motion, such as stair ascent/descent, cutting, hopping, or single-leg squatting, could reveal additional sequence-dependent discrepancies. Additionally, investigations into how rotation sequence selection impacts downstream metrics (e.g., joint moments, muscle moment arms, and inverse dynamic outputs). Ultimately, community-wide consensus on joint- and motion-specific rotation sequence selection will enhance reproducibility, support *meta*-analyses, and facilitate translation of biomechanical findings into clinical care.

5. Conclusion

This study demonstrates that Cardan sequence selection can significantly influence reported joint kinematics within the ankle joint complex, particularly in the ST and TN joints, which exhibit multiplanar motion and greater DOF. While the ISB-recommended XYZ sequence (DF/PF followed by INV/EV followed by IR/ER) remains appropriate for joints with predominantly planar motion, such as the TT, TaF, and TiF joints, our findings reveal that alternative sequences can produce substantial differences in joints with more complex kinematic behavior. These effects were evident under both *in vivo* biplane fluoroscopy gait analysis and *in vitro* passive joint ROM data from robotic cadaveric simulation, underscoring the sensitivity of ST and TN joint kinematics to rotation order. The main contribution of this study is to highlight the need for careful, joint-specific consideration when selecting Cardan sequences, particularly for hindfoot and midfoot joints, where conventional practices may introduce misinterpretation. Moving toward anatomically informed and motion-specific sequence selection will be essential for improving the consistency, interpretability, and clinical relevance of future foot and ankle biomechanical investigations.

CRediT authorship contribution statement

Anthony H. Le: Writing – review & editing, Writing – original draft, Visualization, Validation, Software, Methodology, Investigation, Formal analysis, Data curation, Conceptualization. **Kassidy Knutson:** Writing – review & editing, Methodology, Data curation. **Andrew C. Peterson:** Writing – review & editing, Software, Data curation. **Bruce A. MacWilliams:** Writing – review & editing, Validation. **Karen M. Kruger:** Writing – review & editing, Validation, Conceptualization. **Amy L. Lenz:** Writing – review & editing, Validation, Supervision, Project administration, Investigation, Funding acquisition, Conceptualization.

Declaration of competing interest

The authors declare that they have no known competing financial interests or personal relationships that could have appeared to influence the work reported in this paper.

Acknowledgment

This study was supported by the National Institutes of Health (NIH NIAMS R01 AR083490).

References

- Aliaj, K., Foreman, K.B., Chalmers, P.N., Henninger, H.B., 2021. Beyond Euler/Cardan analysis: true glenohumeral axial rotation during arm elevation and rotation. *Gait Posture* 88, 28–36.
- Areblad, M., Nigg, B., Ekstrand, J., Olsson, K., Ekström, H., 1990. Three-dimensional measurement of rearfoot motion during running. *J. Biomech.* 23, 933–940.
- Behling, A.-V., Welte, L., Kelly, L., Rainbow, M.J., 2024. Human *in vivo* midtarsal and subtalar joint kinematics during walking, running, and hopping. *J. R. Soc. Interface* 21, 20240074.
- Behling, A.-V., Welte, L., Rainbow, M.J., Kelly, L., 2025. Human *in vivo* talocrural contributions to ankle joint complex kinematics during walking, running, and hopping. *Heliyon* 11.
- Brockett, C.L., Chapman, G.J., 2016. Biomechanics of the ankle. *Orthopaedics Trauma* 30, 232–238.
- Conconi, M., Pompili, A., Sancisi, N., Durante, S., Leardini, A., Belvedere, C., 2024. Foot kinematics as a function of ground orientation and weightbearing. *J. Orthopaedic Res.* 42, 148–163.
- Craig, J.J., 2006. Introduction to Robotics. Pearson Education.
- Crawford, N., Yamaguchi, G., Dickman, C., 1996. Methods for determining spinal flexion/extension, lateral bending, and axial rotation from marker coordinate data: analysis and refinement. *Hum. Mov. Sci.* 15, 55–78.
- De Asla, R.J., Kozañek, M., Wan, L., Rubash, H.E., Li, G., 2009. Function of anterior talofibular and calcaneofibular ligaments during *in-vivo* motion of the ankle joint complex. *J. Orthop. Surg. Res.* 4, 1–6.
- de Asla, R.J., Wan, L., Rubash, H.E., Li, G., 2006. Six DOF *in vivo* kinematics of the ankle joint complex: application of a combined dual-orthogonal fluoroscopic and magnetic resonance imaging technique. *J. Orthop. Res.* 24, 1019–1027.
- Grood, E.S., Suntay, W.J., 1983. A joint coordinate system for the clinical description of three-dimensional motions: application to the knee. *J. Biomech. Eng.* 105, 136–144.
- Henry, J.K., Hoffman, J., Kim, J., Steineman, B., Sturnick, D., Demetracopoulos, C., Deland, J., Ellis, S., 2022. The foot and ankle kinematics of a simulated progressive collapsing foot deformity during stance phase: a cadaveric study. *Foot Ankle Int.* 43, 1577–1586.
- Imsdahl, S.I., Stender, C.J., Cook, B.K., Pangrazzi, G., Patthanacharoenphon, C., Sangeorzan, B.J., Ledoux, W.R., 2020. Anteroposterior translational malalignment of ankle arthrodesis alters foot biomechanics in cadaveric gait simulation. *J. Orthop. Res.* 38, 450–458.
- Ito, K., Hosoda, K., Shimizu, M., Ikemoto, S., Kume, S., Nagura, T., Imanishi, N., Aiso, S., Jinzaki, M., Oghara, N., 2015. Direct assessment of 3D foot bone kinematics using biplanar X-ray fluoroscopy and an automatic model registration method. *J. Foot Ankle Res.* 8, 21.
- Kessler, S.E., Rainbow, M.J., Lichtwark, G.A., Cresswell, A.G., D'Andrea, S.E., Konow, N., Kelly, L.A., 2019. A direct comparison of biplanar videoradiography and optical motion capture for foot and ankle kinematics. *Front. Bioeng. Biotechnol.* 7, 199.
- Knutson, K., Muhrad, E.P., Peterson, A.C., Leonard, T., Anderson, A.M., Aragon, K.C., Eatough, Z.J., MacWilliams, B.A., Kruger, K.M., Lenz, A.L., 2024. Talar and calcaneal coordinate axes definitions across foot pathologies. *J. Biomech.* 175, 112298.
- Kobayashi, T., Suzuki, E., Yamazaki, N., Suzukawa, M., Akaike, A., Shimizu, K., Gamada, K., 2015. *In vivo* talocrural joint contact mechanics with functional ankle instability. *Foot Ankle Spec.* 8, 445–453.
- Kozañek, M., Rubash, H.E., Li, G., de Asla, R.J., 2009. Effect of post-traumatic tibiotalar osteoarthritis on kinematics of the ankle joint complex. *Foot Ankle Int.* 30, 734–740.

- Le, A.H., Peterson, A.C., Rodríguez, J.A.L., Miyamoto, T., Nickisch, F., Lenz, A.L., 2025. Passive ankle and hindfoot kinematics within a robot-driven tibial movement envelope. *J. Biomech.* 112740.
- Ledoux, W.R., 2023. Role of robotic gait simulators in elucidating foot and ankle pathomechanics. *Foot Ankle Clin.*
- Lenz, A., Strobel, M.A., Anderson, A.M., Fial, A.V., MacWilliams, B.A., Krzak, J.J., Kruger, K.M., 2021. Assignment of local coordinate systems and methods to calculate tibiotalar and subtalar kinematics: a systematic review. *J. Biomech.* 110344.
- Lundberg, A., Svensson, O., 1993. The axes of rotation of the talocalcaneal and talonavicular joints. *Foot* 3, 65–70.
- Lundgren, P., Nester, C., Liu, A., Arndt, A., Jones, R., Stacoff, A., Wolf, P., Lundberg, A., 2008. Invasive in vivo measurement of rear-, mid-and forefoot motion during walking. *Gait Posture* 28, 93–100.
- MacWilliams, B.A., Davis, R.B., 2013. Addressing some misperceptions of the joint coordinate system. *J. Biomech. Eng.* 135, 54506.
- Maharaj, J.N., Rainbow, M.J., Cresswell, A.G., Kessler, S., Konow, N., Gehring, D., Lichtwark, G.A., 2022. Modelling the complexity of the foot and ankle during human locomotion: the development and validation of a multi-segment foot model using biplanar videoradiography. *Comput. Methods Biomed. Eng.* 25, 554–565.
- Muhirad, E.P., Peterson, A.C., Anderson, A.M., Aragon, K.C., Lisonbee, R.J., MacWilliams, B.A., Kruger, K.M., Lenz, A.L., 2024. Recommendation of minimal distal tibial length for long axis coordinate system definitions. *J. Biomech.* 170, 112153.
- Natsakis, T., Burg, J., Dereymaeker, G., Jonkers, I., Vander Sloten, J., 2016. Foot–ankle simulators: a tool to advance biomechanical understanding of a complex anatomical structure. *Proc. Inst. Mech. Eng. [H]* 230, 440–449.
- Nester, C., Bowker, P., Bowden, P., 2002. Kinematics of the midtarsal joint during standing leg rotation. *J. Am. Podiatr. Med. Assoc.* 92, 77–81.
- Nester, C., Jones, R.K., Liu, A., Howard, D., Lundberg, A., Arndt, A., Lundgren, P., Stacoff, A., Wolf, P., 2007a. Foot kinematics during walking measured using bone and surface mounted markers. *J. Biomech.* 40, 3412–3423.
- Nester, C., Liu, A., Ward, E., Howard, D., Cocheba, J., Derrick, T., 2010. Error in the description of foot kinematics due to violation of rigid body assumptions. *J. Biomech.* 43, 666–672.
- Nester, C., Liu, A., Ward, E., Howard, D., Cocheba, J., Derrick, T., Patterson, P., 2007b. In vitro study of foot kinematics using a dynamic walking cadaver model. *J. Biomech.* 40, 1927–1937.
- Nester, C.J., Findlow, A., Bowker, P., 2001. Scientific approach to the axis of rotation at the midtarsal joint. *J. Am. Podiatr. Med. Assoc.* 91, 68–73.
- Nichols, J.A., Roach, K.E., Fiorentino, N.M., Anderson, A.E., 2017. Subject-specific axes of rotation based on talar morphology do not improve predictions of tibiotalar and subtalar joint kinematics. *Ann. Biomed. Eng.* 45, 2109–2121.
- Nichols, T.E., Holmes, A.P., 2002. Nonparametric permutation tests for functional neuroimaging: a primer with examples. *Hum. Brain Mapp.* 15, 1–25.
- Novacheck, T.F., 1998. The biomechanics of running. *Gait Posture* 7, 77–95.
- Okita, N., Meyers, S.A., Challis, J.H., Sharkey, N.A., 2009. An objective evaluation of a segmented foot model. *Gait Posture* 30, 27–34.
- Pataky, T.C., 2010. Generalized n-dimensional biomechanical field analysis using statistical parametric mapping. *J. Biomech.* 43, 1976–1982.
- Pataky, T.C., Robinson, M.A., Vanrenterghem, J., 2013. Vector field statistical analysis of kinematic and force trajectories. *J. Biomech.* 46, 2394–2401.
- Pataky, T.C., Robinson, M.A., Vanrenterghem, J., 2016. Region-of-interest analyses of one-dimensional biomechanical trajectories: bridging 0D and 1D theory, augmenting statistical power. *PeerJ* 4, e2652.
- Pataky, T.C., Vanrenterghem, J., Robinson, M.A., 2015. Zero-vs. one-dimensional, parametric vs. non-parametric, and confidence interval vs. hypothesis testing procedures in one-dimensional biomechanical trajectory analysis. *J. Biomech.* 48, 1277–1285.
- Peeters, K., Natsakis, T., Burg, J., Spaepen, P., Jonkers, I., Dereymaeker, G., Vander Sloten, J., 2013. An in vitro approach to the evaluation of foot-ankle kinematics: performance evaluation of a custom-built gait simulator. *Proc. Inst. Mech. Eng. [H]* 227, 955–967.
- Perez, K.N., Peterson, A.C., Lisonbee, R.J., Loan, J.P., Lenz, A.L., 2024. Cadaveric validation of markerless tracking using weightbearing computed tomography versus conventional computed tomography imaging techniques. *Med. Eng. Phys.* 134, 104252.
- Peterson, A.C., Kruger, K.M., Lenz, A.L., 2023. Automatic anatomical foot and ankle coordinate toolbox. *Front. Bioeng. Biotechnol.* 11.
- Phadke, V., Braman, J.P., LaPrade, R.F., Ludewig, P.M., 2011. Comparison of glenohumeral motion using different rotation sequences. *J. Biomech.* 44, 700–705.
- Sammacco, V.J., 2004. The talonavicular and calcaneocuboid joints: anatomy, biomechanics, and clinical management of the transverse tarsal joint. *Foot Ankle Clin.* 9, 127–145.
- Sarrafian, S.K., 1993. Biomechanics of the subtalar joint complex. *Clin. Orthop. Relat. Res.* 1976–2007 (290), 17–26.
- Schache, A.G., Wrigley, T.V., Blanch, P.D., Starr, R., Rath, D.A., Bennell, K.L., 2001. The effect of differing Cardan angle sequences on three dimensional lumbo-pelvic angular kinematics during running. *Med. Eng. Phys.* 23, 495–503.
- Sinclair, J., Hebron, J., Hurst, H., Taylor, P., 2013. The influence of different Cardan sequences on three-dimensional cycling kinematics. *Human Movement* 14, 334–339.
- Sinclair, J., Taylor, P.J., Edmundson, C.J., Brooks, D., Hobbs, S.J., 2012. Influence of the helical and six available Cardan sequences on 3D ankle joint kinematic parameters. *Sports Biomech.* 11, 430–437.
- Thewlis, D., Richards, J., Hobbs, S.J., 2008. The appropriateness of methods used to calculate joint kinematics. *J. Biomech.* 41, S320.
- Tweed, J.L., Campbell, J., Thompson, R., Curran, M., 2008. The function of the midtarsal joint: a review of the literature. *Foot* 18, 106–112.
- Wahl, E.P., Lin, W.D., Whittaker, E.C., Cook, B.K., Sangeorzan, B.J., Ledoux, W.R., 2024. Normal and malaligned talonavicular fusion alters cadaveric foot pressure and kinematics. *J. Orthopaedic Res.*
- Wang, B., Roach, K.E., Kapron, A.L., Fiorentino, N.M., Saltzman, C.L., Singer, M., Anderson, A.E., 2015. Accuracy and feasibility of high-speed dual fluoroscopy and model-based tracking to measure in vivo ankle arthrokinematics. *Gait Posture* 41, 888–893.
- Whittaker, E.C., Aubin, P.M., Ledoux, W.R., 2011. Foot bone kinematics as measured in a cadaveric robotic gait simulator. *Gait Posture* 33, 645–650.
- Wu, G., Cavanagh, P.R., 1995. ISB recommendations for standardization in the reporting of kinematic data. *J. Biomech.* 28, 1257–1261.
- Wu, G., Siegler, S., Allard, P., Kirtley, C., Leardini, A., Rosenbaum, D., Whittle, M., D'Lima, D.D., Cristofolini, L., Witte, H., Schmid, O., Stokes, I., 2002. ISB recommendation on definitions of joint coordinate system of various joints for the reporting of human joint motion—part I: ankle, hip, and spine. *J. Biomech.* 35, 543–548.